

Aeroacoustics of Three-Stream High-Speed Jets from Coaxial and Asymmetric Nozzles

Dimitri Papamoschou,* Andrew D. Johnson,† and Vincent Phong‡
University of California, Irvine, Irvine, California 92697

DOI: 10.2514/1.B35130

The development of three-stream variable-cycle turbofan engines for tactical aircraft provides an opportunity for noise reduction by shaping the exhaust of the secondary and tertiary streams. The paper reviews an experimental study of subscale three-stream jets operating at high specific thrust and issuing from rapid-prototyped nozzles. Exhaust conditions at four set points, with variable tertiary pressure ratio and bypass ratio, were determined using thermodynamic cycle analysis. Nozzles were fabricated for each set point and featured coaxial and non-coaxial exit geometries. The operating conditions were simulated using precisely metered helium–air mixtures, and far-field noise surveys were collected using a 24-microphone array. For a low-bypass ratio, a coaxial configuration offers no significant noise benefit compared to the single-stream primary jet. Configurations with offset secondary or tertiary streams offer significant noise reduction in the direction of the thicker flow. For an overall bypass ratio around 0.5, reductions of 5.1 dB in overall sound pressure level and 4.2 dB in effective perceived noise level were attained.

Nomenclature

A	=	exit area
f	=	frequency
p	=	pressure
Sk	=	skewness
T	=	temperature
U	=	fully expanded velocity
γ	=	specific heat ratio
θ	=	polar angle
ϕ	=	azimuth angle

Subscripts

p	=	primary
s	=	secondary
t	=	tertiary
0	=	total
∞	=	ambient

I. Introduction

THE problems of understanding, modeling, and reducing turbulent mixing noise from high-speed jets have occupied the aeroacoustics community for over five decades. Initial motivation was the noise from early jetliners propelled by low-bypass engines, as well as the supersonic Concorde, which was powered by pure turbojets with very high specific thrust [1]. As subsonic jetliners became quieter with the development of the high-bypass turbofan, research on high-speed jet noise was directed toward the development of the high-speed civil transport (HSCT), a supersonic commercial airliner. The HSCT effort resulted in significant progress on the fundamental and applied aspects of the problem [2], although the

aircraft concept was eventually deemed economically unfeasible and the project was terminated. Today, research on high-speed jet noise is primarily motivated by the need for tactical supersonic aircraft to become more environmentally acceptable. A related aspect is the exposure of carrier-deck personnel to extremely high sound pressure levels, which can cause hearing loss and other adverse health effects [3]. Solutions for tactical aircraft are bound to benefit future supersonic business jets that have similar operational characteristics. An important consideration in current and future efforts is the advent of the variable-cycle engine, which allows control of the bypass ratio and features two- and three-stream architectures. The three-stream implementation is the focus of the present study.

Noise reduction concepts for high-speed jets have taken many forms and have generated a large body of literature. A comprehensive review can be found in a recent paper by Morris and McLaughlin [4]. Here, we focus on fundamental concepts and associated noise reduction methods pertaining to multistream jets. It is first important to recognize that, at high exhaust velocities associated with tactical aircraft engines, the dominant noise source is Mach wave radiation: the sound generated by the supersonic convection of the large-scale turbulent eddies in the jet plume. In addition, shock-associated noise can be significant if the jet is not pressure matched, but it is typically not as strong as Mach wave radiation. Therefore, suppression of Mach wave radiation is essential for achieving the desired reductions in community noise and carrier-deck noise. Research on supersonic coaxial jets started in the 1970s, with initial emphasis on reduction of shock-cell noise [5]. Significant theoretical, computational, and experimental work followed [6–11], with the models by Tanna and Morris [7] and Fisher et al. [8] offering perhaps the most insightful look into the differences between the coaxial jet and the single-stream jet. In particular, these models recognized that sound generation from the inner shear layer is suppressed as long as the inner shear layer is surrounded by the outer potential core. The noise suppression is related to the decrease in the turbulence level due to the reduced shear and to the lower relative (convective) Mach number of the eddies, which results in lower radiation efficiency. In a related finding, Papamoschou [12] noticed suppression of Mach waves when a supersonic jet was enveloped with a lower-speed secondary flow. For practical low-bypass configurations, however, the secondary core ends far upstream of the primary core, so most of the primary shear layer is not enveloped by the secondary potential core. Therefore, noise reduction in coaxial jets (compared to the primary stream alone) is marginal unless the secondary to primary nozzle exit diameter ratio is large [13].

The beneficial effect of the secondary flow (namely, the reduced sound generation from the primary shear layer) can be extended further downstream by inducing an asymmetry in the nozzle and/or

Presented as Paper 2013-0007 at the 51st AIAA Aerospace Sciences Meeting, Grapevine, TX, 7–10 January 2013; received 13 August 2013; revision received 28 January 2014; accepted for publication 28 January 2014; published online 12 May 2014. Copyright © 2014 by D. Papamoschou. Published by the American Institute of Aeronautics and Astronautics, Inc., with permission. Copies of this paper may be made for personal or internal use, on condition that the copier pay the \$10.00 per-copy fee to the Copyright Clearance Center, Inc., 222 Rosewood Drive, Danvers, MA 01923; include the code 1533-3876/14 and \$10.00 in correspondence with the CCC.

*Professor, Department of Mechanical and Aerospace Engineering; dpapamos@uci.edu. Fellow AIAA.

†Postdoctoral Fellow, Department of Mechanical and Aerospace Engineering; adjohnso@uci.edu. Member AIAA.

‡Graduate Student Researcher, Department of Mechanical and Aerospace Engineering; vphong@uci.edu. Student Member AIAA.

the jet plume that concentrates the secondary flow in the azimuthal direction where noise reduction is desired. Asymmetry in the nozzle entails offsetting the primary and secondary ducts, whereas asymmetry in the jet plume (issuing from a coaxial arrangement) can be induced by placing deflectors in the secondary stream. These “offset-stream” approaches have been investigated for supersonic [14–17] and subsonic [17–20] jets. The acoustic benefit at supersonic speed can be quite substantial, whereas it is more moderate at subsonic speed.

Reynolds-averaged Navier–Stokes (RANS) computations [17,20,21] have consistently shown a reduction in turbulent kinetic energy (TKE) on the side of the jet with thicker secondary flow. Experiments at moderate scale by Zaman [16], using hot-wire probes, also showed a reduction in turbulence intensity on the thickened side of the jet. Tests at large scale by Brown et al. [19], using particle image velocimetry, did not show a reduction in TKE, possibly because the baseline jet in those tests had a small degree of asymmetry. Acoustic analogy modeling by Papamoschou and Rostamimonjezi [17] showed that a reduction in TKE itself does not explain the far-field noise reduction measured experimentally; equally or more important is the decline in radiation efficiency of the most energetic eddies because of the reduced convective Mach number of those eddies.

A past method that bears an external resemblance to the offset-stream approach is the thermal acoustic shield wherein a layer of low-velocity gas surrounds the principal jet and provides a refractive/reflective layer between the jet noise sources and the ground-based observer [2,22,23]. Applications considered full or partial coverage of the jet. The reliance on refraction and reflection differentiates the physics of the thermal acoustic shield from the physics of the offset-stream approach previously discussed. In addition, the thermal acoustic shield was typically treated as an “add-on” to the engine exhaust system, whereas the offset-stream approach is considered as integrated with the engine cycle.

The variable-cycle turbofan engine has the potential to address the competing demands of tactical aircraft missions for low bypass at supersonic cruise and high bypass at subsonic speeds. The three-stream double-bypass architecture is particularly attractive from the point of view of optimization and operational flexibility [24]. A notional diagram of a three-stream turbofan architecture is shown in Fig. 1; the figure includes only elements that will be used in a basic cycle analysis to be presented later. Implementation on practical engines is more elaborate, and the reader is advised to consult [24] for further details. In addition to its thermodynamic benefits, the third stream can be used for additional purposes such as cooling and lift augmentation. At optimal conditions, the third stream is delivered at a higher-bypass ratio and lower fan pressure ratio than the second stream [24]. This results in a relatively large tertiary exit area, which provides an opportunity for tailoring the initial profile of the third stream for noise reduction. Coaxial three-stream acoustic experi-

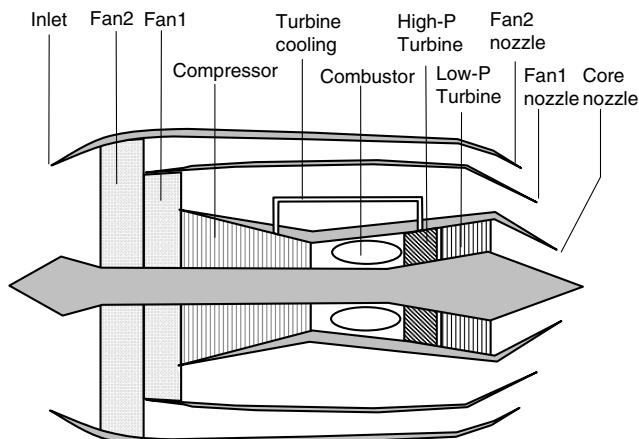


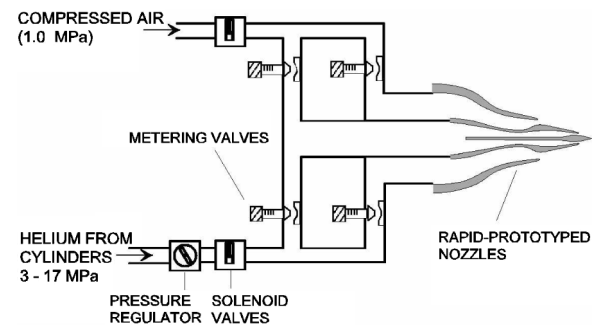
Fig. 1 Notional three-stream turbofan.

ments by Henderson [25] were conducted at subsonic exhaust conditions and at bypass ratios around 5. Introduction of the third stream at a velocity lower than that of the secondary stream moderately reduced high-frequency noise. On an equal-thrust basis, there was no acoustic benefit of the three-stream jet over the two-stream jet. However, the area ratio of the tertiary stream was moderate and larger areas could prove beneficial. The results of Henderson’s study are consistent with the dual- versus single-jet experience when the secondary area is not large enough for the outer flow to substantially envelop the primary core.

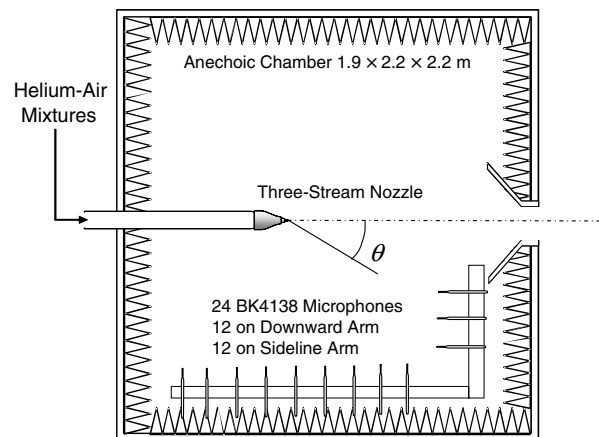
The present study investigates the acoustics of three-stream jets at higher-specific thrust conditions than those studied in the past [25], with emphasis on the effects of nozzle asymmetry motivated by the earlier two-stream research previously cited. The exhaust conditions are determined by thermodynamic cycle analysis of the three-stream configuration shown in Fig. 1, using parameter values thought to represent the state of the art in current or near-future military engines. Several cycles and nozzle geometries are investigated, including coaxial and asymmetric nozzle configurations. Of particular interest is whether the low-speed condition of the tertiary stream, inherent in the three-stream architecture, can provide Mach wave suppression from the very fast primary stream.

II. Conceptual Design of the Nozzle

The objective of the nozzle design process was to generate test models that would enable rapid and accurate testing of a variety of nozzles having characteristics compatible with the cycles of high-performance jet engines. The nozzles needed to fit the capacity of the University of California, Irvine (UCI) jet aeroacoustics facility depicted in Fig. 2. This is a dual-stream jet facility that delivers helium–air mixtures to the primary (core) and secondary (fan) flows of the nozzle. Helium–air mixtures accurately simulate the acoustics and fluid mechanics of hot jets [26,27]. To accommodate a third stream, the supply of the third stream is the same as that of the second



a)



b)

Fig. 2 Jet aeroacoustics facility: a) dual-stream apparatus; and b) microphone array setup inside anechoic chamber.

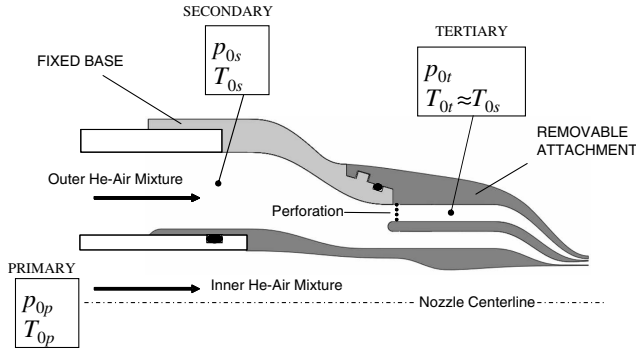


Fig. 3 Conceptual design of three-stream nozzle.

stream with a pressure drop device to independently control the total pressure of the third stream. The resulting conceptual nozzle design is shown in Fig. 3. The pressure drop for the tertiary stream is enabled by a perforated plate mounted at the entrance of the tertiary duct. The nozzle incorporates a fixed base section and removable attachment parts that include the variable-geometry portions of the nozzle.

The sub-millimeter tolerance requirements for the nozzle exit motivated a design where all the nozzle components are built in one piece, using high-definition stereolithography. The design comprises a fixed base on which a variety of nozzle attachments can be mounted, as illustrated in Fig. 3. When the attachment is secured to the base, the primary nozzle is supplied by an independently regulated helium-air mixture. An O-ring fitting prevents leakage to the outer streams. The secondary and tertiary streams are fed by a second helium-air mixture. The supply is bisected in the attachment section with a perforated screen placed at the entrance of tertiary reservoir to control the tertiary total pressure, which is always lower than the secondary total pressure. The details of the nozzle design are reviewed in Sec. IV.

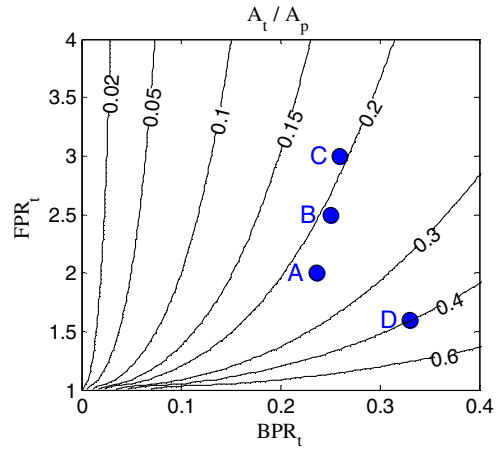
III. Engine Cycles Simulated

The cycle model is based on classic treatments in thermodynamic textbooks [28] combined with additional information published in recent literature, including the cooling of the high-pressure turbine with air bled by the compressor [15,29,30]. Predictions of the model have agreed fairly well with published data on the performance of existing dual-stream engines. Figure 1 shows the principal elements of the three-stream gas turbine engine. The engine parameters were calibrated to give exhaust conditions that reasonably represent a modern high-performance low-bypass engine. This resulted in a turbine rotor inlet temperature (RIT) equal to 2100 K, an overall pressure ratio of 50 (OPR), and turbine cooling using 22.5% of the core mass flow extracted at the exit of the compressor. Power extraction from the turbine to run auxiliary system was set at 2%. These parameters were fixed in the engine cycle analysis.

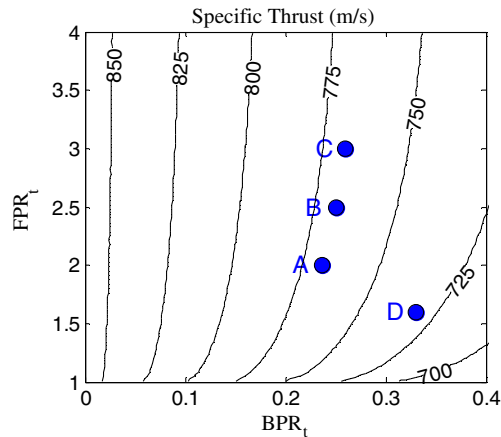
Parametric studies of the engine cycle were conducted at fixed secondary bypass ratio ($BPR_s = 0.26$) and fixed overall fan pressure ratio ($FPR = 4.67$). The tertiary bypass ratio (BPR_t) and the tertiary fan pressure ratio (FPR_t ; extracted from the overall fan pressure ratio) were variable. Table 1 summarizes the fixed and variable parameters of the engine cycle analysis. Increasing the tertiary fan pressure ratio

Table 1 Engine cycle parameters

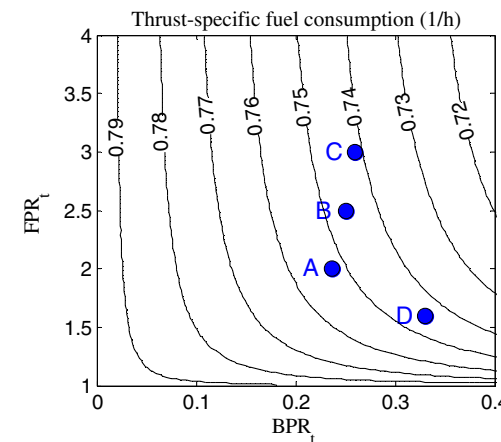
Parameter	Value
Overall pressure ratio	50
Turbine inlet temperature (RIT)	2100 K
Core bleed air fraction for turbine cooling	0.225
Overall fan pressure ratio ($FPR = FPR_s$)	4.67
Secondary bypass ratio BPR_s	0.26
Tertiary fan pressure ratio FPR_t	Variable
Tertiary bypass ratio BPR_t	Variable



a)



b)



c)

Fig. 4 Cycle analysis results versus tertiary bypass ratio and tertiary fan pressure ratio: a) tertiary-to-primary exit area ratio specific thrust; b) specific thrust; and c) thrust-specific fuel consumption.

FPR_t or the tertiary bypass ratio BPR_t results in a decline of the primary exhaust conditions (Mach number, velocity) because more power is extracted from the core flow. For fixed secondary fan pressure ratio and secondary bypass ratio, the secondary exhaust conditions experience very minor variations and remain virtually fixed at $A_s/A_p \approx 0.165$ and $U_s/U_p \approx 0.65$.

The variation of key engine parameters and exhaust conditions are examined in the form of contour plots versus FPR_t and BPR_t . Figure 4 plots the tertiary-to-primary exit area ratio (A_t/A_p), specific thrust, and thrust-specific fuel consumption. The location of four cycle points of this study (A, B, C, and D) are marked. Cycles A, B, and C are on a constant specific-thrust line and increasing FPR_t .

Cycle D is a higher-BPR_t, lower-FPR_t, set point. For noise reduction, particularly with offset-stream configurations, the area ratio A_t/A_p is a critical parameter because it governs the extent of the secondary core that suppresses turbulence levels and reduces the convective Mach number. Cycle D has $A_t/A_p = 0.4$, roughly double that of the other cycles.

The use of helium–air mixtures enables exact matching of the exit velocity and Mach number, with slight deviations in the density ratio [26]. The total temperatures T_0 and nozzle temperature ratios (NTRs) ($NTR = T_0/T_\infty$, where T_∞ is the ambient static temperature) used in this paper refer to equivalent temperatures, simulated using the helium–air mixtures. Equivalent temperature is defined here as the temperature of a hot jet that produces the same velocity as the helium–air mixture jet, at the Mach number of the helium–air mixture jet. Because the helium–air mixture has a specific heat ratio γ higher than air, the nozzle pressure ratio (NPR) for a particular Mach number is slightly different from that for air.

A constraint in the nozzle design of Fig. 3 was the common supply for the secondary and tertiary streams. Adjustment (reduction) in the total pressure of the tertiary stream was enabled by a restriction in the form of a perforated plate at the entrance of the tertiary nozzle. Consequently, the total temperature of the tertiary stream was controlled by that of the secondary stream. This relation is an exact equality for the actual total temperatures and an approximate equality ($T_{0t} \approx T_{0s}$) for equivalent total temperatures, using helium–air mixtures, because of the effects of the variable γ . The ramification of this aspect of the design (the total temperature of the tertiary stream being set by that of the secondary stream) is that one cannot match both the velocity and the Mach number of the tertiary stream. The selection here was to match the velocity as it is more pertinent to acoustics. Because the tertiary stream was “warmer” than its nominal cycle condition, it was run at a lower NPR (lower Mach number) than the cycle point in order to match the velocity. In summary, the nozzle setup enabled the following simulation of the cycle conditions: the velocity and Mach number of the primary stream were both matched; the velocity and Mach number of the secondary stream were both matched; and the velocity of the tertiary stream was matched, but the tertiary Mach number was slightly lower than the cycle point. This resulted in moderately lower tertiary bypass ratio and nozzle pressure ratio compared to the actual cycle point.

Table 2 lists the conditions simulated experimentally for the four cycle points of Fig. 4. The primary exit velocity ranges between 887 and 910 m/s. The secondary exhaust velocity is practically constant at about 584 m/s. The tertiary velocity varies significantly for each cycle and is as low as 284 m/s for cycle D. The ratio of primary thrust over total thrust was 0.78, 0.77, 0.75, and 0.78 for cycles A, B, C, and D, respectively. For all cycles, the helium mass fraction of the primary flow was near 0.6 and the specific heat ratio γ was around 1.6. For the secondary and tertiary flows, the helium mass fraction was 0.10 and $\gamma = 1.49$.

IV. Detailed Nozzle Design and Fabrication

A. Design

The subscale nozzle was designed to be compatible with existing flow rate capabilities of the UCI jet aeroacoustics facility. Since the majority of mass flow is needed to supply the primary flow, the primary exit diameter was the driving dimension for the scaling process. Based on past experiments with supersonic helium–air mixtures [9], an exit diameter of 18.28 mm (0.72 in.) was deemed appropriate. The lip thickness of the nozzle was limited by the manufacturing process and

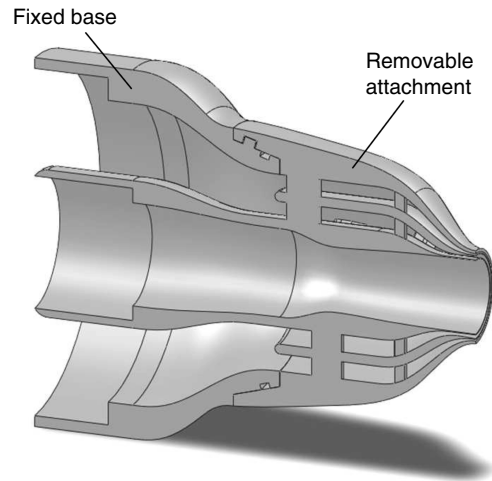


Fig. 5 Cutaway view of nozzle.

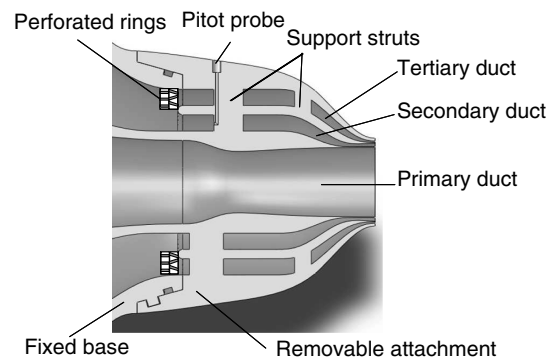


Fig. 6 Nozzle section showing internal structure and total pressure measurement.

the resulting structural integrity of the nozzle walls. These constraints led to a thickness of 0.203 mm (0.008 in.)

The expansion part of the primary duct was designed using the method of characteristics (MOC) for uniform exit flow and included the effect of the displacement thickness of the boundary layer [31]. Each nozzle was designed so that the primary stream exited at pressure-matched conditions at the respective conditions listed in Table 2. The design Mach numbers for cycles A, B, C, and D were 1.613, 1.596, 1.578, and 1.593, respectively. Upstream of the throat, the contour in the subsonic region was defined by a fifth-order polynomial that provided the desired fit between inlet and throat sections. Given the very small dimensions of the secondary duct, an MOC method was deemed unnecessary and the entire contour was defined by fifth-order polynomials that provided the correct exit-to-throat area ratio. The tertiary nozzle, entirely subsonic, was also defined by fifth-order polynomials. All of the ducts terminated with zero slope. Because the secondary and tertiary nozzles had large contraction ratios, the inlet flow was very low subsonic, allowing the placement of support struts without disturbing the exit flow.

The coordinates of the nozzles were imported into Solidworks (Dassault Systemes) and integrated into a CAD model with fixed

Table 2 Set points based on experimental simulation of engine cycle

Case	Primary			Secondary					Tertiary				
	NPR	NTR	U_p , m/s	BPR _s	NPR _s	NTR _s	U_s/U_p	A_s/A_p	BPR _t	NPR _t	NTR _t	U_t/U_p	A_t/A_p
A	4.50	4.13	905	0.26	4.67	1.65	0.645	0.168	0.13	1.69	1.62	0.396	0.215
B	4.39	4.11	895	0.26	4.67	1.65	0.652	0.166	0.15	2.13	1.62	0.470	0.193
C	4.28	4.08	887	0.26	4.67	1.65	0.659	0.164	0.17	2.60	1.62	0.529	0.180
D	4.59	4.08	910	0.26	4.67	1.65	0.641	0.164	0.24	1.45	1.62	0.313	0.398

Table 3 Nozzle specifications^a

Nozzle	Description	Exit dimensions in millimeters (Figs. 7 and 8)				
		A	B	C	D	E
A	Cycle A: all streams coaxial	18.29	0.72	0.84	—	—
B	Cycle B: all streams coaxial	18.29	0.72	0.76	—	—
C	Cycle C: all streams coaxial	18.29	0.72	0.72	—	—
D	Cycle D: all streams coaxial	18.29	0.72	1.51	—	—
AE	Cycle A: eccentric tertiary duct	18.29	0.72	1.68	0.00	—
CE	Cycle C: eccentric tertiary duct	18.29	0.72	1.40	0.00	—
DE	Cycle D: eccentric tertiary duct	18.29	0.72	3.02	0.00	—
DEX	Cycle d: eccentric ellipsoidal tertiary duct	18.29	0.72	2.76	0.00	—
DEX2	Cycle D: eccentric ellipsoidal tertiary duct and eccentric secondary duct	18.28	1.44	2.76	0.00	0.00

^aA = Diameter of primary (inner) duct; B = thickness of secondary-duct annulus (maximum thickness for eccentric configuration); C = thickness of tertiary-duct-annulus (maximum thickness for eccentric configuration); D = minimum thickness of tertiary-duct annulus; and E = minimum thickness of secondary-duct annulus.

portions comprising the interface with the base section and internal support struts. A cutaway view of the CAD model of one of the coaxial nozzles is shown in Fig. 5. Figure 6 shows a cross-sectional view with instrumentation to be discussed next. The overall length of the assembly was 114.3 mm, and the maximum diameter at the base is 95.0 mm. The interface between the base and the attachment used a notch and key style locking mechanism. The nozzle was secured in place by rotating the attachment piece with respect to the base. An O ring situated in a groove on the base section ensured a leak-free internal flow. The pressure drop for the tertiary stream was controlled using two back-to-back perforated rings, as shown in Fig. 6. The hole pattern on each ring allowed precise flow control by clocking the

rings. The rings were interlocking and the combination of the two rings sat firmly at the entrance of the tertiary nozzle.

B. Total Pressure Measurement

The primary total pressure was measured by inserting a pitot probe in the upstream supply of the primary stream. Measurement of the secondary and tertiary total pressures presented a bigger challenge because of the split shown in Fig. 3 and the overall complexity of the nozzle. Inserting pitot tubes into the secondary and tertiary streams was deemed impractical. Instead, the total pressure measurement was integrated into the design of the nozzle by including pressure ports in the internal support struts. Very thin channels, of 0.75 mm diameter,

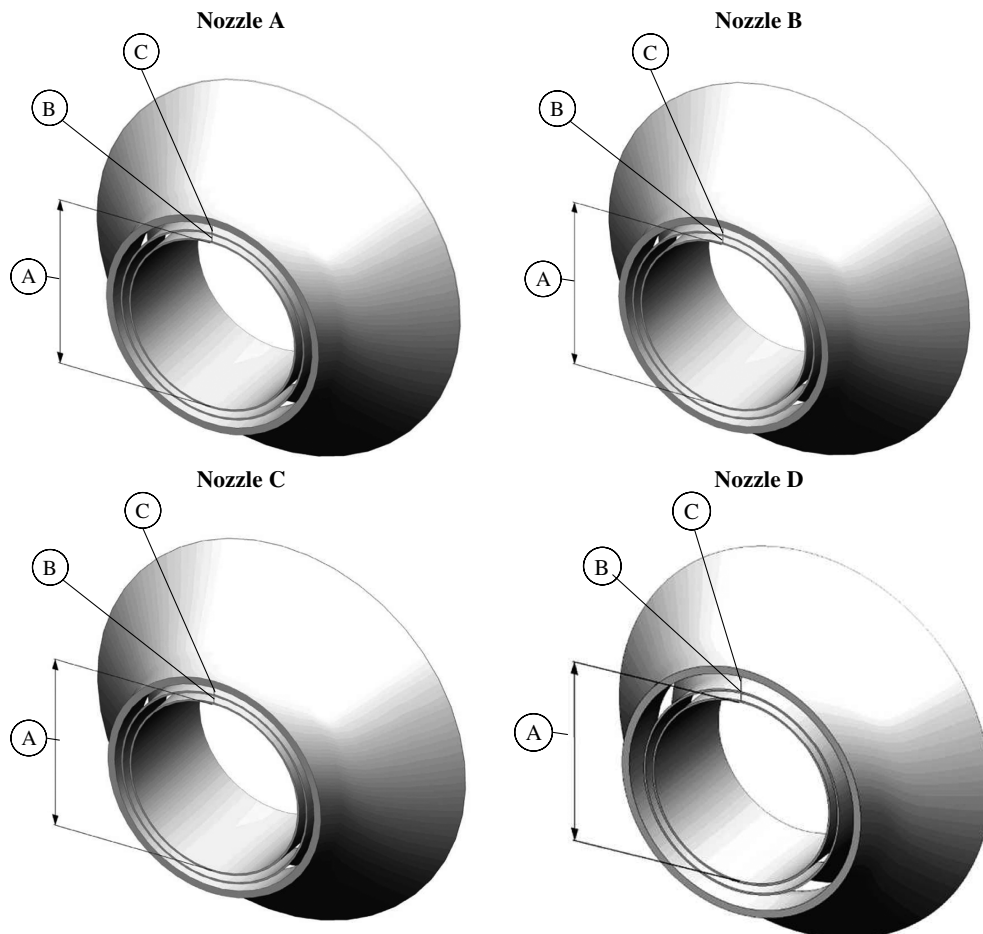


Fig. 7 Coaxial nozzles tested.

were introduced in two of these struts: one to measure the secondary total pressure and the other to measure the tertiary total pressure. The channels began at the outer surface of the attachment, followed an L-shaped path through the struts, and terminated into upstream-facing ports in their respective ducts. The cross-sectional image of Fig. 6 illustrates the secondary pitot port; the tertiary port was similarly arranged.

C. Fabrication

The base and attachment pieces were fabricated using ultrafine resolution stereolithography with build layers of 0.05 mm (FineLine

Prototyping, Inc.) The material used was Accura 60 (3D Systems) with tensile strength of 58–68 MPa and flexural strength of 87–101 MPa. The large flexural strength results in a very rigid structure, even at the thin nozzle lips. Consequently, there was no deformation of the nozzles during testing. The specifications of the nozzles covered in this paper are listed in Table 3. Figures 7 and 8 show the exit shapes for the coaxial and non-coaxial nozzles, respectively. Coaxial configurations were tested at all four cycle points. Nozzles with eccentric circular tertiary duct were tested for cycles A, C, and D. Two additional geometries were tested for cycle D. One had an ellipsoidal eccentric tertiary duct (nozzle DEX), designed to give uniform annulus

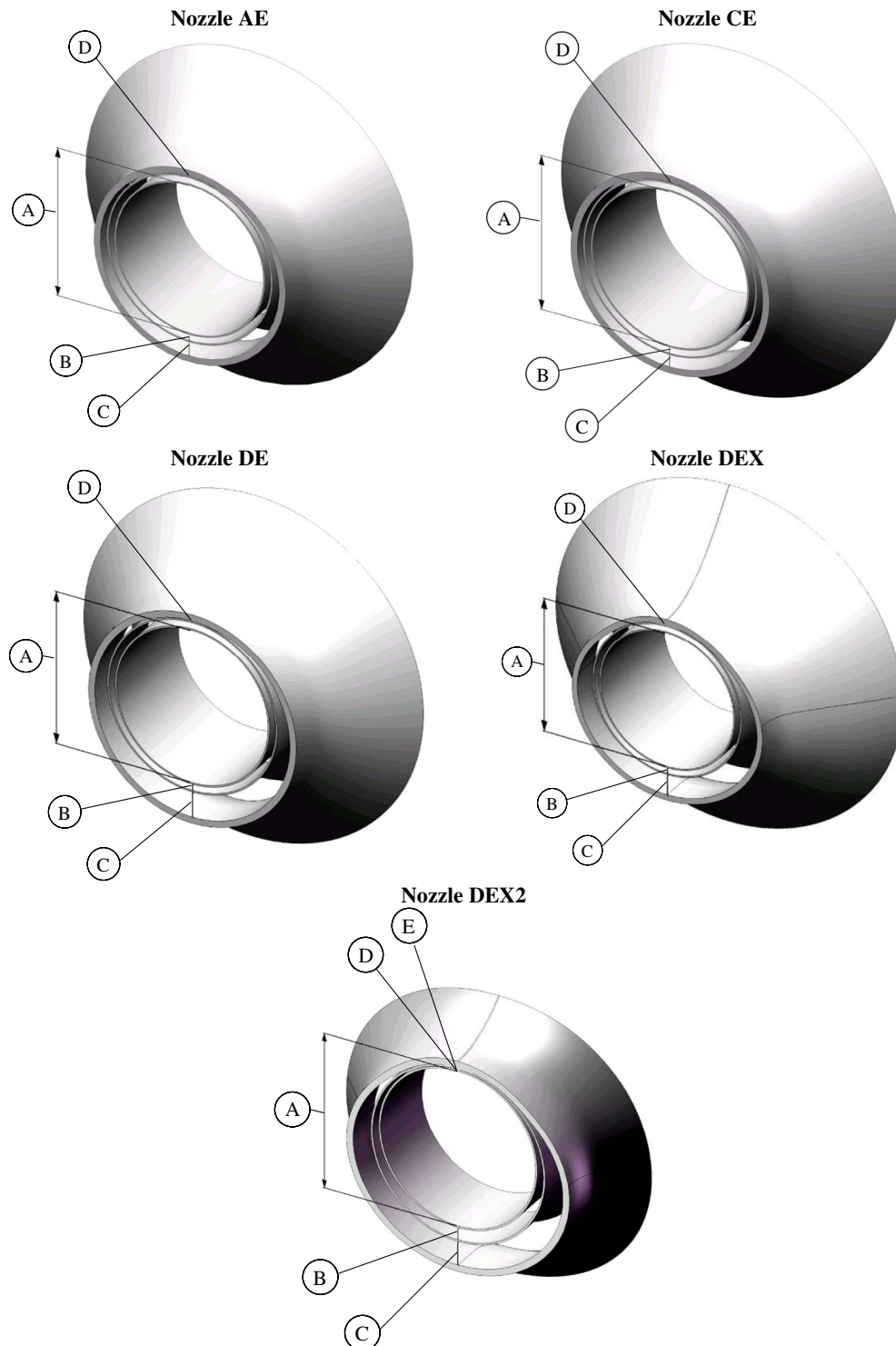


Fig. 8 Eccentric configurations tested.

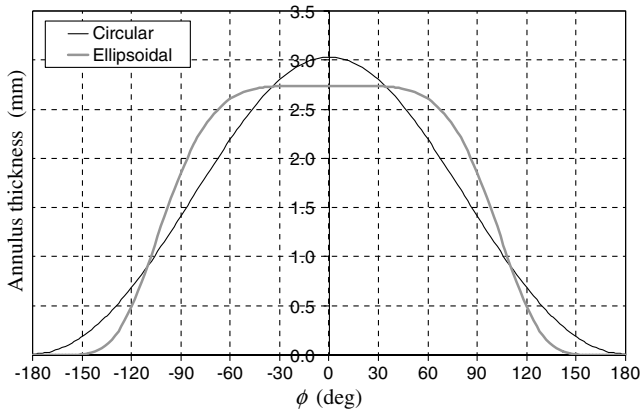


Fig. 9 Azimuthal distribution of annulus thickness for eccentric circular tertiary duct (nozzle DE) and eccentric ellipsoidal tertiary duct (nozzle DEX).

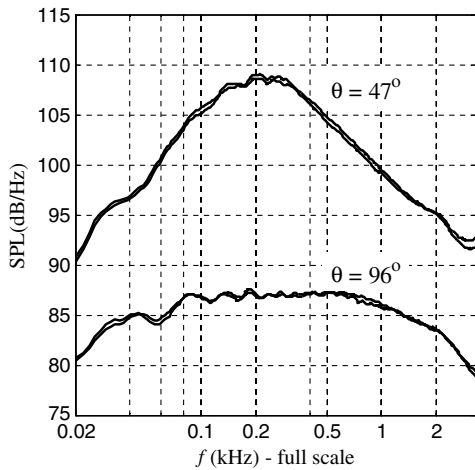


Fig. 10 Narrowband SPL spectra of two repeated tests of case C.

thickness over azimuthal angles $-60 \text{ deg} \leq \phi \leq 60 \text{ deg}$ with respect to the downward direction on the plane of symmetry. The annulus thickness distribution for this nozzle is compared to that of the round

eccentric nozzle in Fig. 9. The other nozzle for cycle D had the same eccentric ellipsoidal tertiary duct as nozzle DEX and included an eccentric round secondary duct (nozzle DEX2).

D. Viscous Effects

Having specified the dimensions of the three-stream nozzles, it is important to evaluate the viscous effects on the nozzle performance. The Reynolds number of the primary stream, based on exit diameter, was near 700,000 for all four cycles. The Reynolds number based on the length of the primary nozzle was 1.3 million; hence, the exit boundary layer was assumed to be turbulent. The nozzle design code by Sivells [31] predicts a displacement thickness of 0.16 mm at the nozzle exit. The associated discharge coefficient is 0.96.

The Reynolds numbers of the coaxial secondary and tertiary streams were evaluated based on their respective exit annulus thicknesses. The Reynolds number of the secondary stream was 42,000 for all four cycles; the Reynolds number of the tertiary stream ranged from 17,000 in cycle A to 25,000 in cycle D. These values are low enough to support laminar boundary layers at the exits of the secondary and tertiary streams. A compressible Thwaites method [32] was used to calculate of the boundary-layer thickness by approximating the annular secondary and tertiary ducts as two-dimensional. The calculated displacement thickness of the secondary flow is 0.024 mm. For the tertiary flow, the displacement thickness ranges from 0.027 mm (cycle C) to 0.036 mm for (cycle D). Note that the rapid contractions in the secondary and tertiary nozzles result in strong favorable pressure gradients, and consequently small displacement thicknesses. The calculated discharge coefficients for the secondary and tertiary nozzles are near 0.95 for all the set points, and are thus similar to the discharge coefficient of the primary nozzle. Therefore, the viscous effects had negligible impact on the inviscid bypass ratios listed in Table 2.

The eccentric arrangements cause additional viscous losses because of the closure of the secondary or tertiary annulus at the top of the nozzle. A thorough evaluation of these losses requires a computation of the flowfield, which was outside the scope of the present work. However, one can attempt a rough calculation by assuming that the segment of the annulus with a thickness less than twice the displacement thickness (evaluated for the coaxial nozzles, as discussed) is completely blocked. This gives a mass flow rate loss between 2 and 3% for all the eccentric configurations considered. The thrust loss is expected to have a similar range. Considering that the secondary and tertiary flows contribute to only ~23% of the total

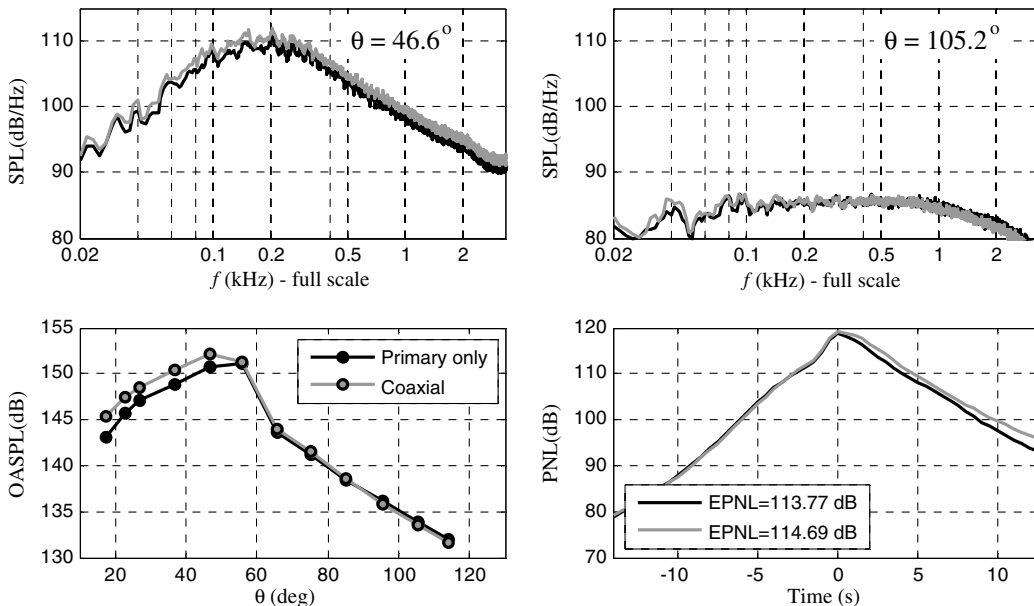


Fig. 11 Acoustic summary for coaxial nozzle A (cycle A). Primary stream alone (black) compared to coaxial three-stream jet (gray). $\Delta\text{OASPL}_{\text{max}} = 1.0 \text{ dB}$; $\Delta\text{EPNL} = 0.9 \text{ dB}$.

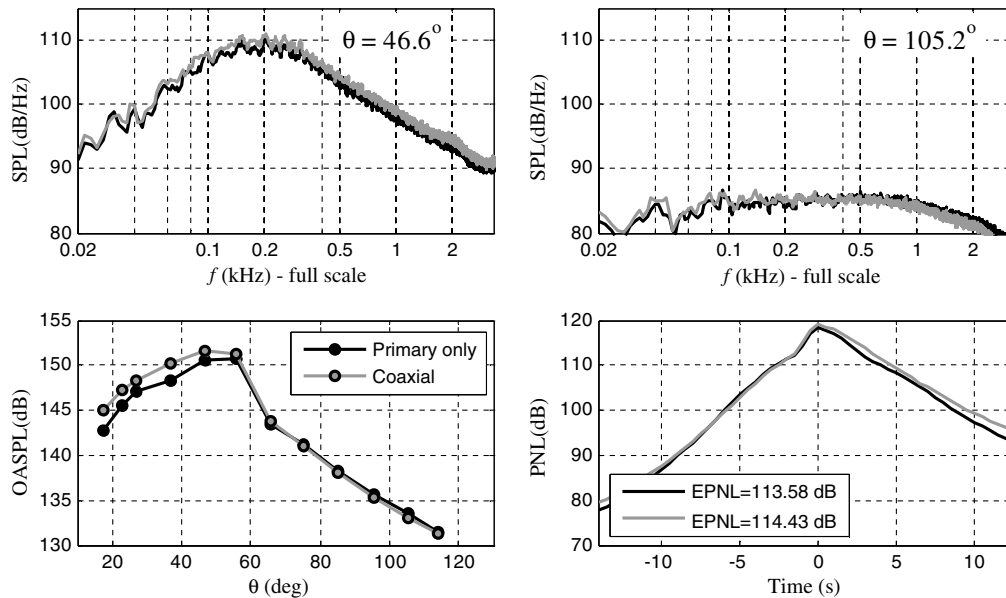


Fig. 12 Acoustic summary for coaxial nozzle B (cycle B). Primary stream alone (black) compared to coaxial three-stream jet (gray). $\Delta\text{OASPL}_{\max} = 0.8$ dB; $\Delta\text{EPNL} = 0.8$ dB.

thrust, a thrust loss of 3% for the secondary and tertiary streams (assuming both are eccentric) translates to a total thrust loss of around 0.6% at static conditions.

V. Aeroacoustic Testing

Noise measurements were conducted in the aeroacoustic facility shown in Fig. 2. The microphone array consists of twenty four $\frac{1}{8}$ -in. condenser microphones (Bruel & Kjaer, model 4138) with a frequency response up to 120 kHz. Twelve microphones were mounted on a downward arm (azimuth angle $\phi = 0$ deg), and 12 were installed on a sideline arm ($\phi = 60$ deg). Figure 2 depicts the configuration of the downward arm; the sideline arm is practically identical. On each arm, the polar angle θ ranged approximately from 20 to 120 deg relative to the downstream jet axis, and the distance to the nozzle exit ranged from 0.916 to 1.234 m. This arrangement

enabled simultaneous measurement of the downward and sideline noise at all the polar angles of interest. The microphones were connected, in groups of four, to six conditioning amplifiers (Bruel & Kjaer, model 2690-A-0S4). The 24 outputs of the amplifiers were sampled simultaneously, at 250 kHz per channel, by three eight-channel multifunction data acquisition boards (National Instruments PCI-6143) installed in a Dell Precision T7400 computer with a Xeon quadcore processor. National Instruments LabView software was used to acquire the signals. The temperature and humidity inside the anechoic chamber were recorded to enable computation of the atmospheric absorption. The microphone signals were conditioned with a high-pass filter set at 300 Hz. Narrowband spectra were computed using a 4096-point fast Fourier transform, yielding a frequency resolution of 61 Hz. The spectra were corrected for microphone actuator response, microphone free-field response, and atmospheric absorption, thus resulting in lossless spectra. For the

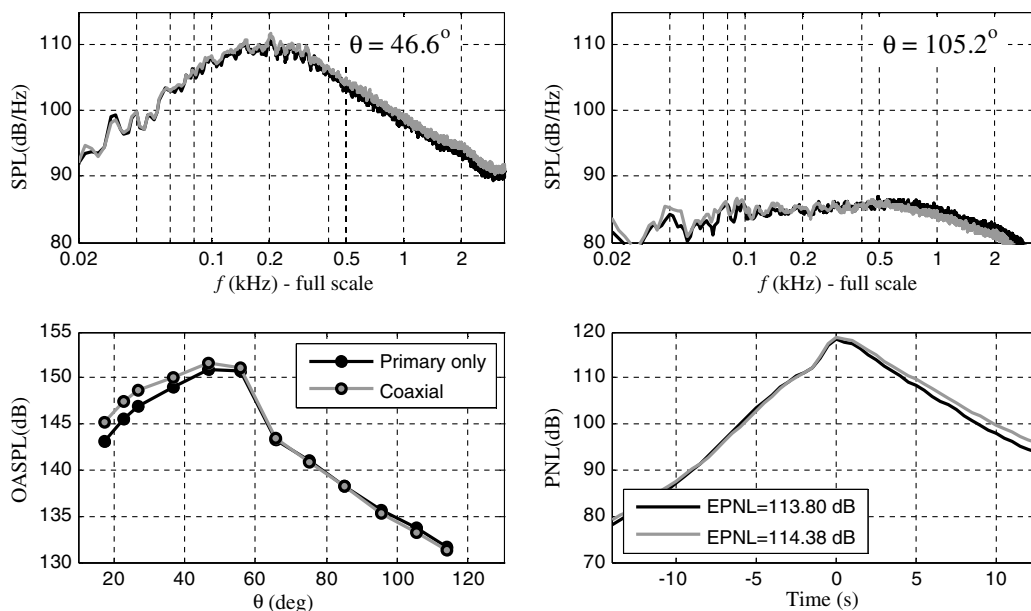


Fig. 13 Acoustic summary for coaxial nozzle C (cycle C). Primary stream alone (black) compared to coaxial three-stream jet (gray). $\Delta\text{OASPL}_{\max} = 0.7$ dB; $\Delta\text{EPNL} = 0.6$ dB.

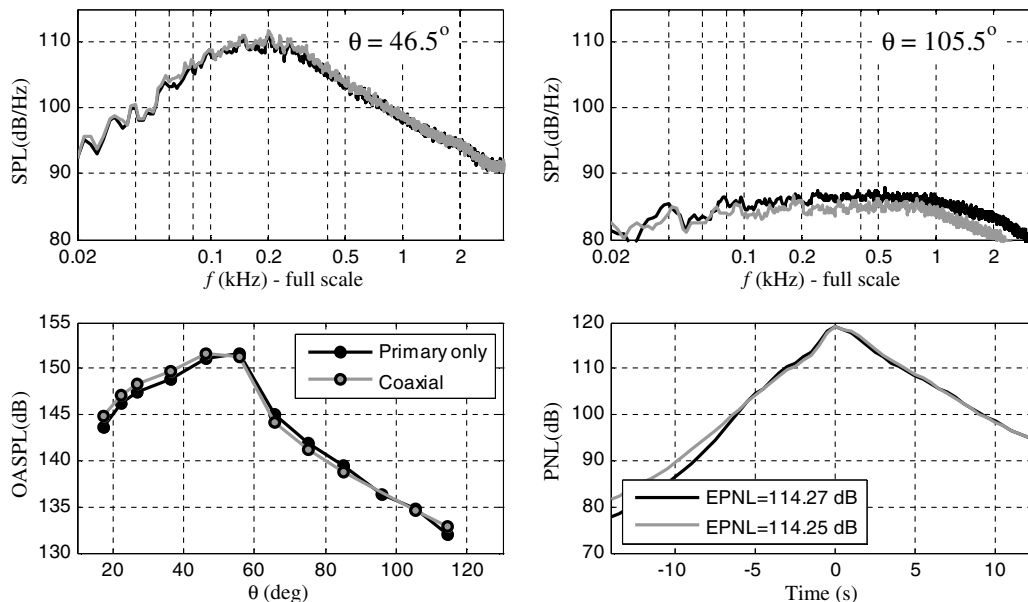


Fig. 14 Acoustic summary for coaxial nozzle D (cycle D). Primary stream alone (black) compared to coaxial three-stream jet (gray). $\Delta\text{OASPL}_{\text{max}} = -0.1$ dB; $\Delta\text{EPNL} = 0.0$ dB.

typical testing conditions of this experiment, and for the farthest microphone location, the absorption correction was 4.5 dB at 120 kHz. Integration of the lossless spectra gave the overall sound pressure level (OASPL).

The flyover perceived noise level (PNL) and effective perceived noise level (EPNL) are used as the primary metrics for evaluating noise reduction. They are calculated based on a full-scale primary diameter of 0.61 m (24 in.) and a flight profile with a Mach number of 0.30, an engine angle of attack of 10 deg, and climb angle of 20 deg. For the “downward” evaluation of EPNL, the observer is on the projection of the flight path on the ground, the airplane altitude directly over the observer is 610 m (2000 ft), and the acoustic measurements at $\phi = 0$ deg are used. For the “sideline” evaluation of EPNL, the observer is offset 450 m from the projection of the flight path, the airplane altitude at the axial position of the observer is 457 m (1500 ft), and the acoustic measurements at $\phi = 60$ deg are used.

Details of the PNL and EPNL calculation procedure are available in [17].

The uncertainty of the acoustic measurements is exemplified in Fig. 10, which plots repeated measurements of the SPL narrowband spectra for nozzle C, with the repeats spaced apart by three months. Two polar angles are presented, $\theta = 47$ deg (peak emission) and $\theta = 96$ deg. For ease of comparison, the spectra were smoothed using a Savitzky–Golay filter. The excellent overlap of the curves is noted. The standard deviation between repeats does not exceed 0.5 dB in sound pressure level (SPL). The resulting variation in the effective perceived noise level is 0.3 dB. Even though repeated measurements were not performed extensively enough for a thorough uncertainty analysis, the aforementioned variations are representative of the repeatability of acoustic measurements in the UCI facility. We also note that the background noise level was at least 20 dB lower than the signal level in all the testing done.

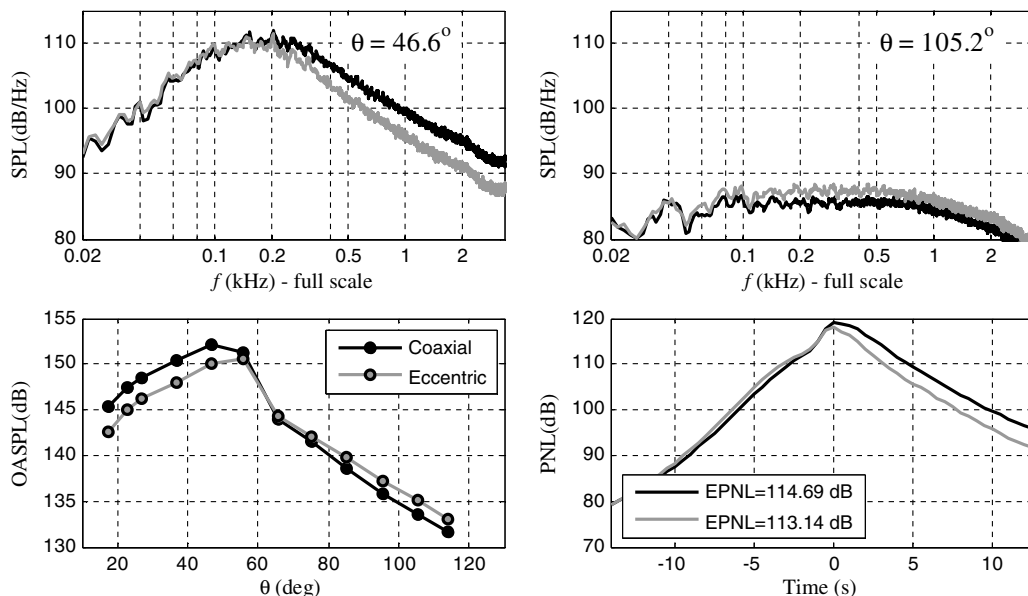


Fig. 15 Acoustic summary for nozzles A and AE (cycle A) in the downward direction. Coaxial jet (black) compared to jet with eccentric tertiary flow (gray). $\Delta\text{OASPL}_{\text{max}} = -1.5$ dB; $\Delta\text{EPNL} = -1.5$ dB.

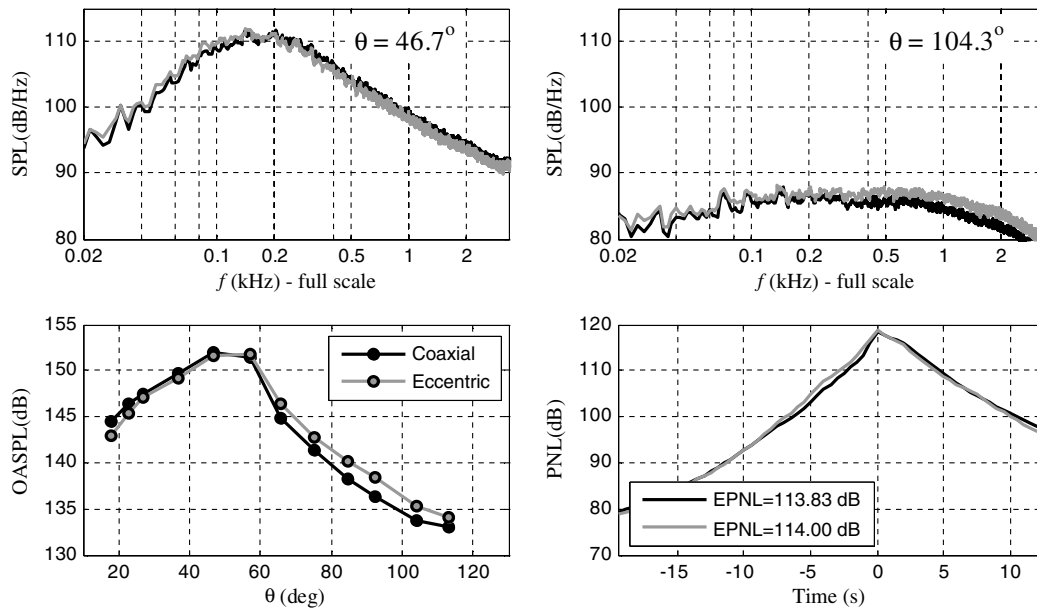


Fig. 16 Acoustic summary for nozzles A and AE (cycle A) in the sideline direction. Coaxial jet (black) compared to jet with eccentric tertiary flow (gray). $\Delta\text{OASPL}_{\max} = -0.1$ dB; $\Delta\text{EPNL} = 0.2$ dB.

The sections that follow will compare the acoustics of single-stream and three-stream coaxial jets, as well as the acoustics of three-stream coaxial and eccentric jets. Because these flows have different thrust levels, one may wish to evaluate the acoustics on an equal-thrust basis. Here, we use simple geometric scaling for far-field acoustics, which gives that the change in decibel level equals 10 times the decimal logarithm of the thrust ratio [12]. Considering that the primary jet generates about 77% of the total thrust, equal-thrust scaling (to the thrust level of the three-stream jet) adds approximately 1.1 dB to the sound pressure level of the primary-only jet. Comparing coaxial and eccentric configurations, the estimated thrust loss of around 0.6% of the eccentric cases (Sec. IV.D) translates to an adjustment of 0.03 dB, which is within the error margin of the experiments.

VI. Results

The acoustic results are presented in two parts. The first part compares the jet with primary flow alone to the three-stream coaxial jet. The purpose of this comparison is to examine the effects of the secondary and tertiary flows, arranged symmetrically, on the acoustic emission. The second part compares the acoustic emission of coaxial and non-coaxial three-stream jets. The comparisons will be provided in terms of an “acoustic summary” comprising the following plots (see Fig. 11, for example): narrowband SPL spectra in the direction of peak emission and at large polar angle; OASPL versus polar angle; and PNL versus flyover time. In addition, estimates of EPNL are shown. For asymmetric nozzles, this information will be provided in the downward ($\phi = 0$ deg) and sideline ($\phi = 60$ deg) azimuthal directions.

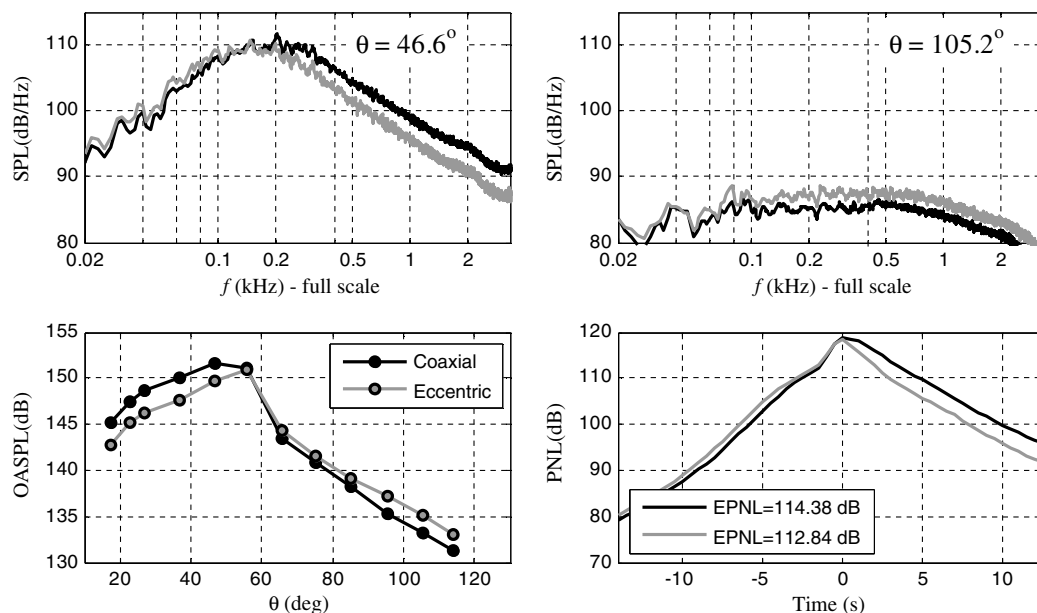


Fig. 17 Acoustic summary for nozzles C and CE (cycle C) in the downward direction. Coaxial jet (black) compared to jet with eccentric tertiary flow (gray). $\Delta\text{OASPL}_{\max} = -0.8$ dB; $\Delta\text{EPNL} = -1.5$ dB.

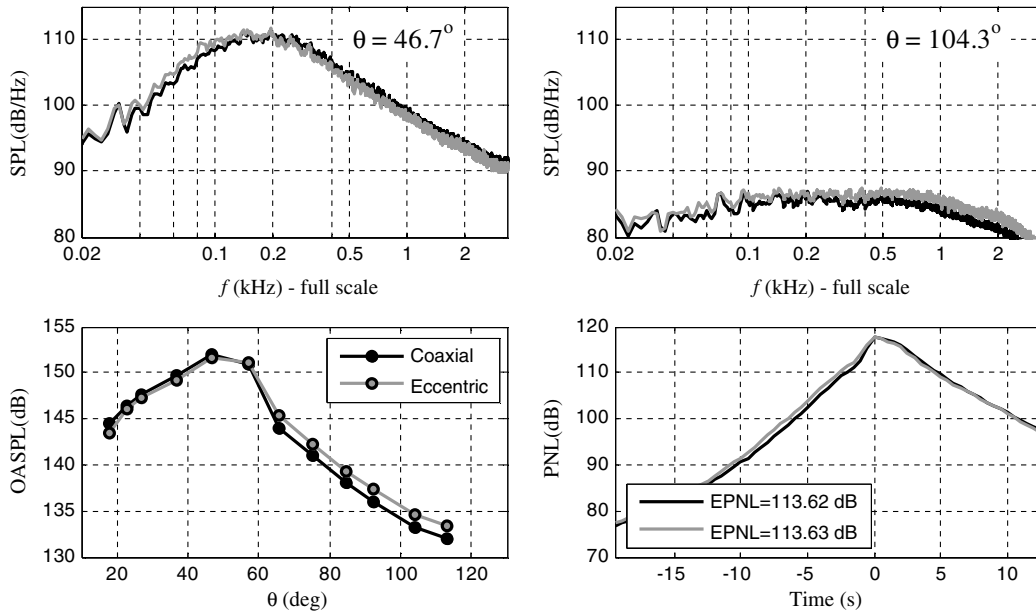


Fig. 18 Acoustic summary for nozzles C and CE (cycle C) in the sideline direction. Coaxial jet (black) compared to jet with eccentric tertiary flow (gray). $\Delta\text{OASPL}_{\text{max}} = -0.3$ dB; $\Delta\text{EPNL} = 0.0$ dB.

A. Three-Stream Coaxial Jet Versus Primary Jet Alone

To assess the potential of Mach wave suppression due to the operating conditions alone, we compare the coaxial three-stream jet with the jet comprising the primary flow alone. Figures 11–14 display the relevant acoustic summaries for cycles A through D. For cycles A, B, and C there are small increases in spectral levels and OASPL at angles lower than the angle of peak emission, followed by no change or a very slight decrease for the larger angles. The overall levels (OASPL, EPNL) increase by about 1 dB. This is on the same order as the noise increase due to the thrust increase associated with the introduction of the secondary and tertiary streams, as explained in Sec. V. We conclude that, for cycles A–C, there is no evidence of noise attenuation by the secondary and tertiary flows. This is due to the very small thicknesses of the secondary and tertiary flows. For cycle D, which has a thicker tertiary flow, we note very

slight increases at the small angles followed by moderate reductions at the large angles. The OASPL and EPNL do not change significantly. On a constant-thrust basis, this flow is ~1 dB quieter, therefore indicating some evidence here of noise suppression due to the reduced shear by the secondary and, particularly, the tertiary streams.

B. Three-Stream Noncoaxial versus Coaxial Jets

Figures 15–20 compare three-stream coaxial jets with three-stream jets having eccentric tertiary duct for cycles A, C, and D. The comparisons now include the downward and sideline azimuthal directions. For cycles A and C, offsetting the tertiary duct causes appreciable reductions in the peak spectral levels in the downward direction, with associated decreases in peak OASPL and EPNL of around 1.5 dB (Figs. 15 and 17). Small increases in SPL and OASPL

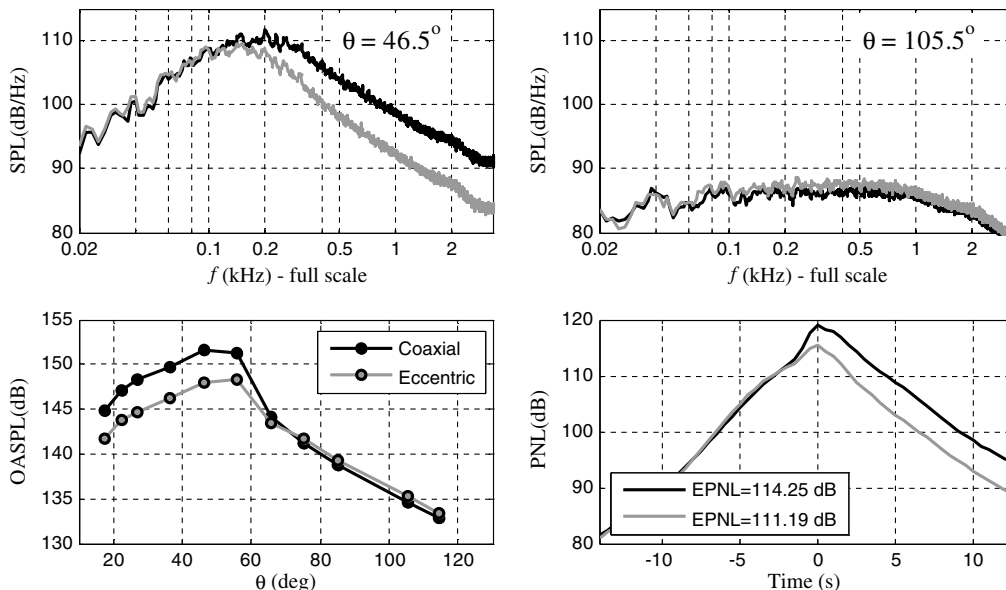


Fig. 19 Acoustic summary for nozzles D and DE (cycle D) in the downward direction. Coaxial jet (black) compared to jet with eccentric tertiary flow (gray). $\Delta\text{OASPL}_{\text{max}} = -3.3$ dB; $\Delta\text{EPNL} = -3.1$ dB.

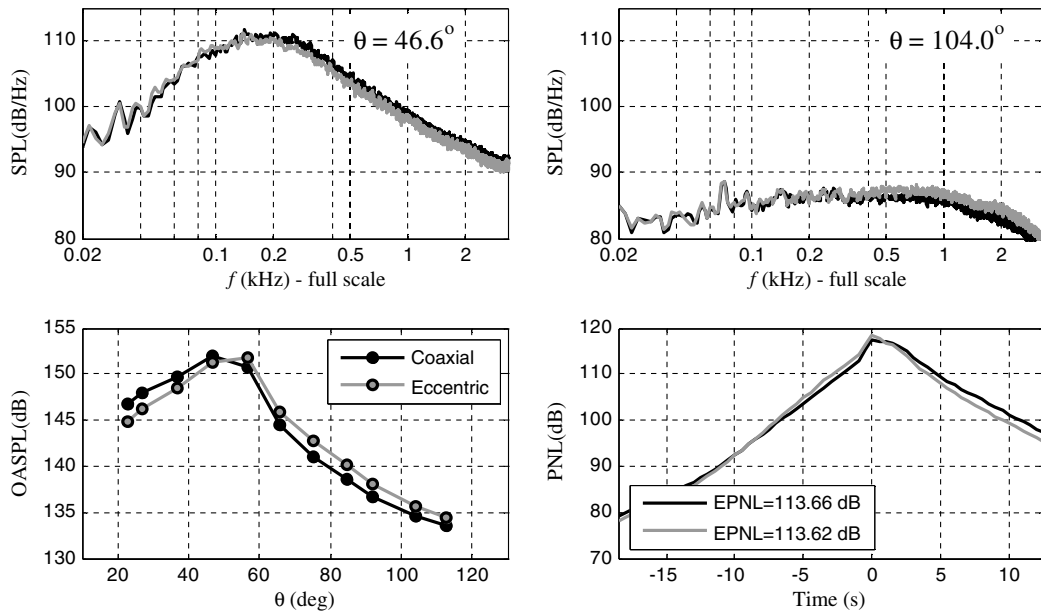


Fig. 20 Acoustic summary for nozzles D and DE (cycle D) in the sideline direction. Coaxial jet (black) compared to jet with eccentric tertiary flow (gray). $\Delta\text{OASPL}_{\text{max}} = -0.2$ dB; $\Delta\text{EPNL} = 0.0$ dB.

are noted for large polar angles. The sideline direction experiences a modest increase in EPNL (cycle A, Fig. 16) or no change (cycle C, Fig. 18). Doubling the tertiary area, cycle D, leads to significant improvements in the downward noise reduction (Fig. 19). The EPNL and peak OASPL both decline by ~ 3 dB. Noise in the sideline direction is practically unchanged (Fig. 20).

The special nozzles DEX and DEX2 are now reviewed in Figs. 21–24. Figure 21 shows that nozzle DEX, with ellipsoidal-eccentric tertiary duct, achieves roughly the same downward reduction as its circular-eccentric counterpart (nozzle DE, Fig. 19). The sideline noise shows a modest improvement over nozzle DE (compare Figs. 20 and 22). This indicates that the approach of increasing the sideline thickness of the tertiary annulus has a benefit on sideline noise, albeit moderate in this design. In nozzle DEX2, the ellipsoidal-eccentric tertiary duct is combined with an eccentric secondary duct, with both eccentricities being directed downward

(Figs. 23 and 24). The combination of the two eccentric ducts offers significant improvements in noise reduction. The downward SPL in the direction of peak emission is reduced by as much as 10 dB at high frequency. The EPNL and peak OASPL reduce by 5.2 and 5.1 dB, respectively, in the downward reduction. This combination also has a distinct benefit in the sideline reduction of 0.9 dB in EPNL and 1.0 dB in peak OASPL.

C. Pressure Skewness

It is well established that the pressure field emitted by high-speed jets contains regions where the waveform is asymmetric, characterized by random occurrences of sharp compressions followed by gradual expansions. The asymmetry can be quantified in terms of the skewness of the pressure or its time derivative. The physical reason for the asymmetry is the steepening of strong nonlinear compression waves emitted by the jet. This phenomenon

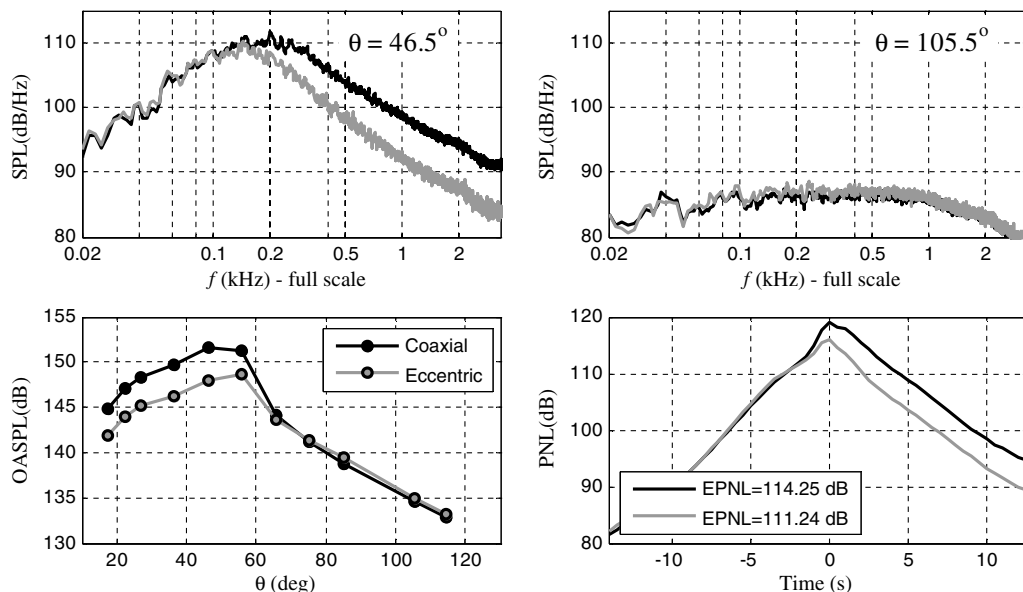


Fig. 21 Acoustic summary for nozzles D and DEX (cycle D) in the downward direction. Coaxial jet (black) compared to jet with eccentric/ellipsoidal tertiary flow (gray). $\Delta\text{OASPL}_{\text{max}} = -2.9$ dB; $\Delta\text{EPNL} = -3.1$ dB.

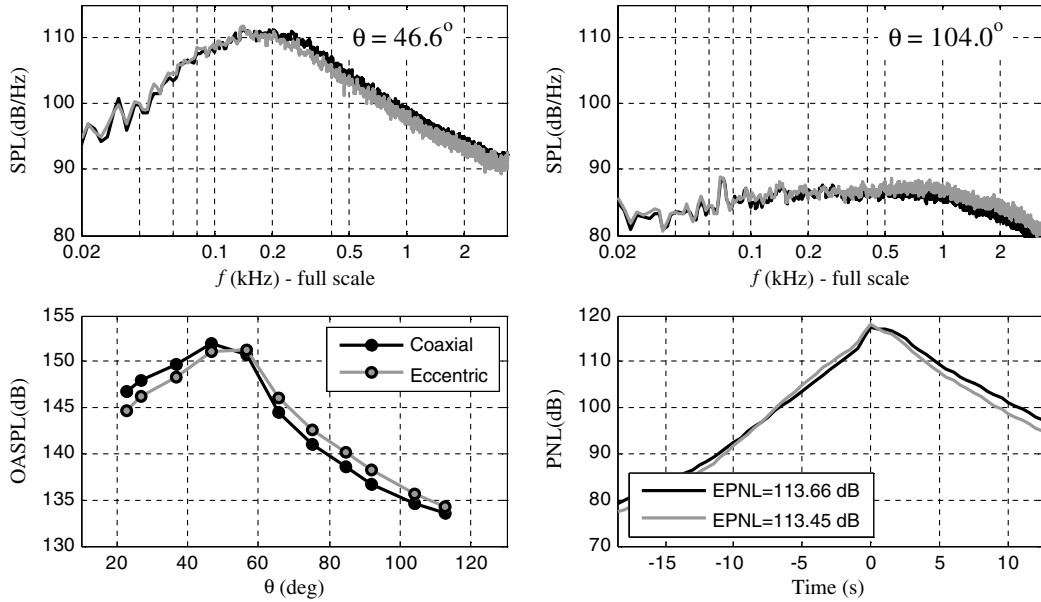


Fig. 22 Acoustic summary for nozzles D and DEX (cycle D) in the sideline direction. Coaxial jet (black) compared to jet with eccentric/ellipsoidal tertiary flow (gray). $\Delta OASPL_{max} = -0.8$ dB; $\Delta EPNL = -0.2$ dB.

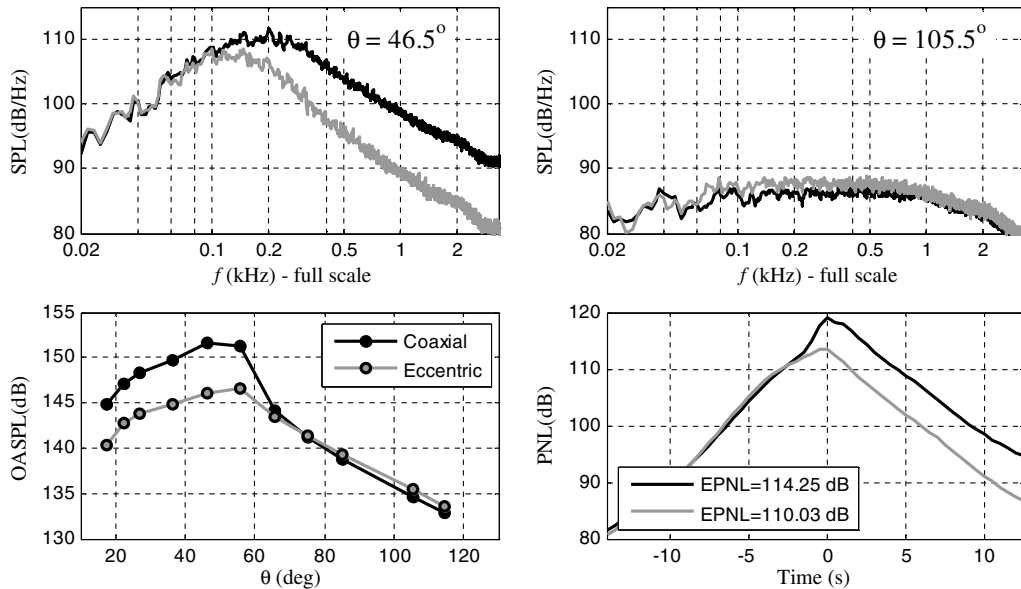


Fig. 23 Acoustic summary for nozzles D and DEX2 (cycle D) in the downward direction. Coaxial jet (black) compared to jet with eccentric/ellipsoidal tertiary flow and eccentric secondary flow (gray). $\Delta OASPL_{max} = -5.1$ dB; $\Delta EPNL = -4.2$ dB.

was connected to “crackle” noise by Ffowcs Williams et al. [33] and has subsequently been the topic of several investigations [14,34–38]. There is strong evidence that the skewness attains large value when the eddy convective Mach number becomes supersonic [33,35]. Therefore, large skewness is intrinsically connected with Mach wave radiation.

We examine the skewness of the pressure field of several of our jets. The skewness is defined as $Sk = \overline{p'^3}$, where p' is the pressure fluctuation and the overbar denotes time averaging. It is presented in the normalized form Sk/σ^3 , where σ is the standard deviation. Figure 25 plots the directivity of the normalized skewness, in the downward azimuthal direction, associated with the following jets at cycle D: primary flow alone; coaxial flow; and eccentric flow from nozzle DEX2. The skewness of the primary-only jet reaches very high value, about 1.6, in the direction of peak emission. Maximization of the skewness in the direction of Mach wave

radiation (direction of peak OASPL), and rapid decline away from this direction, is consistent with the findings of past works. The large peak skewness measured here indicates intense Mach wave radiation, which is expected given the very large jet speeds of this investigation. Addition of the secondary and tertiary flows in a coaxial arrangement (nozzle D) has little effect on the distribution of the skewness. This indicates negligible Mach wave suppression, consistent with the results of Sec. VI.A. On the other hand, the asymmetric addition of secondary and tertiary streams through nozzle DEX2 results in significant suppression of the skewness. The peak value is reduced from 1.6 to 1.0, and values near the angle of peak emission are reduced by as much as 80%. Still, the peak skewness of 1.0 is considerably larger than the “crackle-free” criterion of 0.4 proposed by Ffowcs Williams et al. [33]. This indicates that some Mach wave radiation remains in the DEX2 jet and suggests that there is potential for further noise reduction.

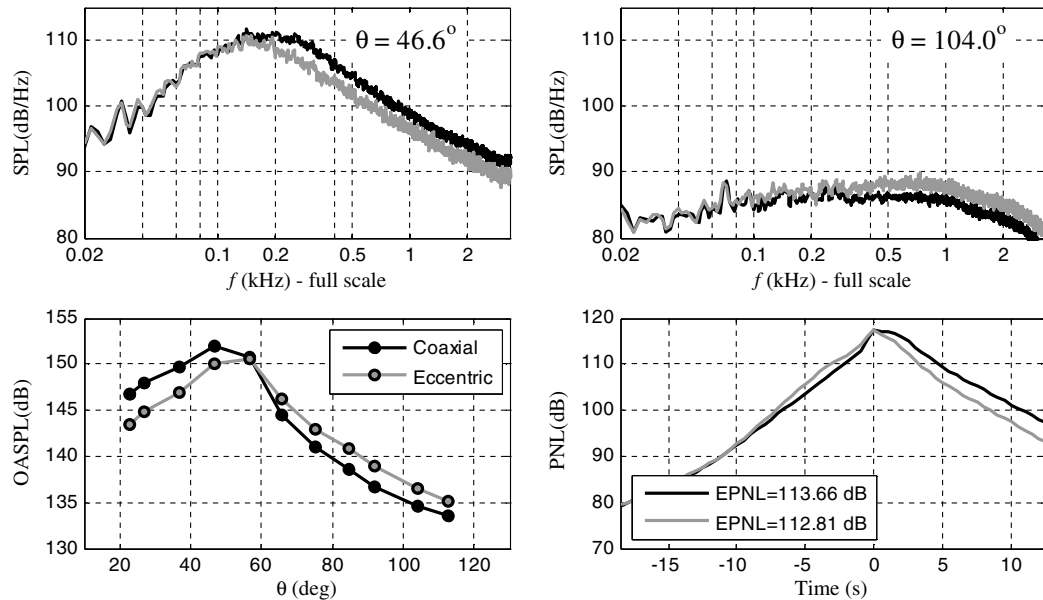


Fig. 24 Acoustic summary for nozzles D and DEX2 (cycle D) in the sideline direction. Coaxial jet (black) compared to jet with eccentric/ellipsoidal tertiary flow and eccentric secondary flow (gray). $\Delta\text{OASPL}_{\text{max}} = -1.3$ dB; $\Delta\text{EPNL} = -0.9$ dB.

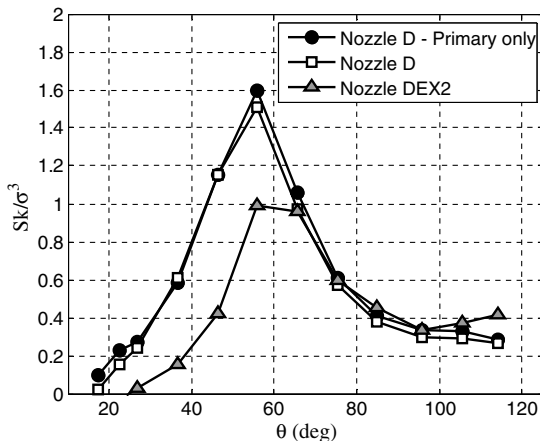


Fig. 25 Directivity of normalized skewness for various jets at cycle D.

VII. Conclusions

The experiments of this study provided an assessment of noise reduction from three-stream high-speed jets by conducting a parametric investigation of round-coaxial and asymmetric nozzles. Relevant cycle conditions were simulated experimentally using intricate subscale nozzles fabricated with advanced stereolithographic methods. The following are the principal findings:

1) For low-bypass-ratio coaxial jets with normal velocity profile, the conditions of the secondary and tertiary streams do not result in significant noise suppression. The annuli of the secondary and tertiary streams are too thin for these flows to penetrate far downstream in order to reduce the Mach wave source of the primary jet.

2) Offset nozzle arrangements offer a significant noise benefit in the direction of the thickened flow, even at moderately low bypass ratios. In jets with an overall bypass ratio around 0.4, an eccentric tertiary stream resulted in noise suppression (over the coaxial configuration) of 1.5 dB in EPNL in the direction of the thickened flow. Increasing the overall bypass ratio to ~ 0.5 improved this figure to ~ 3 dB. It is notable that this reduction was enabled with a tertiary stream supplied at a low pressure ratio and velocity one-third that of the primary stream.

3) The best configuration of this study comprised an eccentric-ellipsoidal tertiary duct combined with an eccentric secondary duct (nozzle DEX2). It provided EPNL reductions of 4.3 dB in the downward direction (direction of thickened flows) and 0.9 dB in the

sideline direction. The peak value of the skewness of the pressure field was reduced by 40% in the downward direction.

4) It is likely that a further increase in the exit area of the tertiary stream will enable even larger noise reductions when using asymmetric nozzle concepts. The associated increase in the tertiary bypass ratio is consistent with advanced engine cycles being proposed for the three-stream turbofan architecture [24]. Increasing the exit area of the secondary stream would be beneficial as well, although the design space there is constrained by the overall fan pressure ratio.

The success of the combined asymmetries in the tertiary and secondary ducts suggests that there is room for further noise reduction, at a fixed bypass ratio, by optimal reshaping of these ducts. This concept may even extend to the primary duct. Optimization would be most effective using a combined experimental and computational effort that illuminates the salient physics of noise suppression. RANS computations coupled with an appropriate acoustic analogy model could help guide experiments toward quiet, practical, and efficient configurations that will address the needs of future supersonic aircraft.

Acknowledgments

We gratefully acknowledge the support by Rolls-Royce, plc., contract RR51848, monitored by William Dalton.

References

- [1] Smith, M. J. T., "Aircraft Noise," Cambridge Univ. Press, Cambridge, England, U.K., 1989, pp. 162–172.
- [2] Seiner, M. J., and Krejsa, E.A., "Supersonic Jet Noise and the High Speed Civil Transport," AIAA Paper 1989-2358, July 1989.
- [3] Aubert, A., and McKinley, R., "Measurements of Jet Noise Aboard US Navy Aircraft Carriers," AIAA Paper 2011-6947, Sept. 2011.
- [4] Morris, P. J., and McLaughlin, D. K., "High Speed Jet Noise Reduction: Past Progress and Future Possibilities," AIAA Paper 2013-0006, Jan. 2013.
- [5] Dosanjh, D., Ahuja, J., Bassiouni, M., and Bhutiani, P., "Supersonic Jet Noise Suppression by Coaxial Cold/Heated Jet Flows," AIAA Paper 1976-507, July 1976.
- [6] Tanna, H. K., "Coannular Jets—Are They Really Quiet and Why?," *Journal of Sound and Vibration*, Vol. 72, No. 1, 1980, pp. 97–118. doi:10.1016/0022-460X(80)90710-5
- [7] Tanna, H. K., and Morris, P. J., "The Noise from Normal-Velocity-Profile Coannular Jets," *Journal of Sound and Vibration*, Vol. 98, No. 2, 1985, pp. 213–234. doi:10.1016/0022-460X(85)90386-4

- [8] Fisher, M. J., Preston, G. A., and Bryce, W. D., "A Modelling of the Noise from Simple Coaxial Jets, Part 1: With Unheated Primary Flow," *Journal of Sound and Vibration*, Vol. 209, No. 3, 1998, pp. 385–403.
- [9] Dahl, M. D., and Papamoschou, D., "Supersonic Coaxial Jets: Noise Predictions and Measurements," *AIAA Journal*, Vol. 38, No. 4, 2000, pp. 584–591.
doi:10.2514/2.1026
- [10] Zaman, K. B. M. Q., and Dahl, M. D., "Noise and Spreading of a Subsonic Coannular Jet: Comparison with Single Equivalent Jet," *AIAA Journal*, Vol. 45, No. 11, 2007, pp. 2661–2670.
doi:10.2514/1.29441
- [11] Bogey, C., Barre, S., Juve, D., and Bailly, C., "Simulation of a Hot Coaxial Jet: Direct Noise Prediction and Flow-Acoustics Correlations," *Physics of Fluids*, Vol. 21, No. 3, 2009, Paper 035105.
doi:10.1063/1.3081561
- [12] Papamoschou, D., "Mach Wave Elimination in Supersonic Jets," *AIAA Journal*, Vol. 35, No. 10, 1997, pp. 1604–1611.
doi:10.2514/2.19
- [13] Papamoschou, D., and Debiassi, M., "Noise Measurements in Supersonic Jets Treated with the Mach Wave Elimination Method," *AIAA Journal*, Vol. 37, No. 2, 1999, pp. 380–387.
doi:10.2514/2.702
- [14] Papamoschou, D., and Debiassi, M., "Directional Suppression of Noise from a High-Speed Jet," *AIAA Journal*, Vol. 39, No. 3, 2001, pp. 380–387.
doi:10.2514/2.1345
- [15] Papamoschou, D., "Engine Cycle and Exhaust Configurations for Quiet Supersonic Propulsion," *AIAA Journal of Propulsion and Power*, Vol. 20, No. 2, 2004, pp. 255–262.
doi:10.2514/1.9251
- [16] Zaman, K. B. M. Q., "Noise- and Flow-Field of Jets from an Eccentric Coannular Nozzle," AIAA Paper 2004-0005, Jan. 2004.
- [17] Papamoschou, D., and Rostamimonjezi, S., "Modeling of Noise Reduction for Turbulent Jets with Induced Asymmetry," AIAA Paper 2012-2158, June 2012.
- [18] Papamoschou, D., "New Method for Jet Noise Suppression in Turbofan Engines," *AIAA Journal*, Vol. 42, No. 11, 2004, pp. 2245–2253.
- [19] Brown, C. A., Bridges, J. E., and Henderson, B., "Offset Stream Technology Test: Summary of Results," AIAA Paper 2007-3664, May 2007.
- [20] Dippold, V., Foster, L., and Wiese, M., "Computational Analyses of Offset-Stream Nozzles for Noise Reduction," *Journal of Propulsion and Power*, Vol. 25, No. 1, 2009, pp. 204–217.
doi:10.2514/1.34943
- [21] DeBonis, J. R., "RANS Analyses of Turbofan Nozzles with Internal Wedge Deflectors for Noise Reduction," *Journal of Fluids Engineering*, Vol. 131, No. 4, 2009, Paper 041104.
doi:10.1115/1.3089536
- [22] Majjigi, R. K., Brausch, J. F., Janardan, B. A., Balsa, T. F., Knott, P. R., and Pickup, N., "Free Jet Feasibility Study of a Thermal Acoustic Shield Concept for AST/VCE Application," NASA CR-3758, July 1984.
- [23] Martens, S., and Haber, L., "Jet Noise Reduction for High-Speed Exhaust Systems," American Soc. of Mechanical Engineers Paper GT2008-50455, Fairfield, NJ, June 2008.
- [24] Simmons, R. J., "Design and Control of a Variable Geometry Turbofan with an Independently Modulated Third Stream," Ph.D. Dissertation, Ohio State Univ., Columbus, OH, 2009.
- [25] Henderson, B., "Aeroacoustics of Three-Stream Jets," AIAA Paper 2012-2159, June 2012.
- [26] Papamoschou, D., "Acoustic Simulation of Coaxial Hot Air Jets Using Cold Helium–Air Mixture Jets," *Journal of Propulsion and Power*, Vol. 23, No. 2, 2007, pp. 375–381.
doi:10.2514/1.21776
- [27] McLaughlin, D. K., Kuo, C. W., and Bridges, J., "On the Scaling of Small, Heat Simulated Jet Noise Measurements to Moderate Size Exhaust Jets," *International Journal of Aeroacoustics*, Vol. 9, Nos. 4–5, 2010, pp. 627–654.
- [28] Hill, P. G., and Peterson, C. R., "Mechanics and Thermodynamics of Propulsion," 2nd ed., Addison-Wesley, Boston, 1992, pp. 157–172.
- [29] Young, J. B., and Wilcock, R. C., "Modeling the Air-Cooled Gas Turbine: Part 1, General Thermodynamics," *Journal of Turbomachinery*, Vol. 124, No. 2, 2002, pp. 207–313.
- [30] Brear, M. J., Kerrebrock, J. L., and Epstein, A. H., "Propulsion System Requirements for Long Range, Supersonic Aircraft," *Journal of Fluids Engineering*, Vol. 128, No. 2, 2005, pp. 370–377.
- [31] Sivells, J. C., "A Computer Program for the Aerodynamic Design of Axisymmetric and Planar Nozzles for Supersonic and Hypersonic Wind Tunnels," U.S. Air Force Arnold Engineering Development Center Rept. AEDC-TC-78-63, Arnold AFB, TN, 1978.
- [32] Rott, N., and Crabtree, L.F., "Simplified Laminar Boundary-Layer Calculations for Bodies of Revolution and for Yawed Wings," *Journal of the Aeronautical Sciences*, Vol. 19, No. 8, 1952, pp. 553–565.
- [33] Williams, F. F. E., Simson, J., and Virchis, V. J., "'Crackle': An Annoying Component of Jet Noise," *Journal of Fluid Mechanics*, Vol. 71, No. 2, Sep. 1975, pp. 251–271.
- [34] Krothapalli, A., Venkatakrishnan, L., and Lourenco, L., "Crackle: A Dominant Component of Supersonic Jet Mixing Noise," AIAA Paper 2000-2024, June 2000.
- [35] Petitjean, B. P., and McLaughlin, D. K., "Experiments on the Nonlinear Propagation of Noise from Supersonic Jets," AIAA Paper 2003-3127, May 2003.
- [36] Mora, P., Heeb, N., Kastner, J., and Gutmark, E. J., "Effect of Scale on the Far-Field Pressure Skewness and Kurtosis of Heated Supersonic Jets," AIAA Paper 2013-0016, Jan. 2013.
- [37] Baars, J. W., Tinney, C. E., and Wochner, M. S., "Nonlinear Noise Propagation from a Fully-Expanded Mach 3 Jet," AIAA Paper 2012-1177, Jan. 2012.
- [38] Gee, K. L., Neilsen, T. B., Downing, J. M., James, M. M., McKinley, R. L., McKinley, R. C., and Wall, T. C., "Near-Field Shock Formation in Noise Propagation from a High-Power Jet Aircraft," *Journal of the Acoustical Society of America*, Vol. 133, No. 2, 2013, pp. EL88–EL93.
doi:10.1121/1.4773225

J. Powers
Associate Editor